Fibers and Polymers 2020, Vol.21, No.4, 690-700
DOI 10.1007/s12221-020-9482-y

ISSN 1229-9197 (print version)
ISSN 1875-0052 (electronic version)

Microcrystalline Cellulose Management in the Production of Poly(ether-urethane)s- Structure, Morphology, and Thermal Characteristic

Paulina Kasprzyk, Kamila Błażek, and Janusz Datta*

Department of Polymers Technology, Faculty of Chemistry, Gdańsk University of Technology, Gdańsk 80-233, Poland
(Received May 8, 2019; Revised July 25, 2019; Accepted September 10, 2019)

Abstract: In response to the demand of polymer industry for reducing the use of synthetic chemicals, eco-friendly materials are investigated. In the presented study, bio-based poly(ether-urethane)s were prepared by using microcrystalline cellulose (MCC) and polyether polyol and 1,3-propanediol derived from corn sugar. A step towards sustainability was taken by incorporating bio-based compounds and cellulose, consequently, bio-waste are utilized in a smart way. The new materials were synthesized via prepolymer method, while the cellulose fibers were added after the reaction. Structural studies of bio-composites were realized by FTIR technique. The number of free and hydrogen-bonded carbonyl groups was determined based on the deconvolution of C=O band. Crystallinity was assessed on the basis of X-ray diffraction analysis. The influence of the MCC content on the thermo-mechanical, thermal and selected mechanical properties has been demonstrated. Results obtained by SEM method showed that the higher degree of reinforcement led to the formation of aggregates reflecting their poor dispersion in the polymer matrix. It may probably result from the relatively weaker interaction between MCC and PU matrix. On the other hand, it was found that the incorporation of fibers improved the thermo-mechanical and thermal properties of the prepared materials. This work provides an effective way of using bio-renewable chemicals in the polyurethane industry without using additional processing apparatus and chemical processes. The used method makes it possible to obtain materials with high bio-content and satisfactory thermal characteristic.

Keywords: Microcrystalline cellulose, Poly(ether-urethane)s, Polyurethanes

Introduction

In recent times, a growing interest in polymer materials obtained from bio-based resources has been noted. The intensity of this trend is driven by the difficulties with the waste disposal, harmful environmental effects of non-renewable resources use, depletion of petroleum-based resources, and by the potential replacement of synthetic substrates without decreasing the properties of a final product [1,2].

Generally, the synthesis of polyurethanes is conducted using one- or two-step (called prepolymer) method [3]. The reaction is realized using aliphatic or aromatic diisocyanates, macrodiols and low molecular weight chain extenders (diamines or diols). According to the available literature, the prospects for the synthesis of polyurethanes and their composites by using bio-based substrates are promising [4,5]. Most of the reviewed scientific papers describe polyurethane materials produced from polyols derived from sugars and modified vegetable oils, such as palm oil [6], rapeseed oil [7,8], castor oil [9], karanja oil [10], soybean oil [11], hemp seed oil [12], canola oil [13], cottonseed oil as well as sorbitol [14] and polyglycerol [15]. The increasing interest in the topic of bio-based chain extenders for the polyurethane synthesis has also been observed, e.g. 1,3-propanediol from Sorghum [16], crude glycerol [17], 1,4-butanediol obtained via Genomatica's process [18], and Zamea® and Susterra® propanediol produced by DuPont Tate & Lyle BioProducts [19]. Recently, scientists have become interested in synthesizing bio-based diisocyanates derived from triglycerides, fatty acids (derivatives of triglycerides) [20,21] or lysine [22].

With reference to the exhausting resources of fossil feedstocks and the need to protect the environment, novel bio-glycol derived from natural resources were proposed as a green alternative substrate for the synthesis. 1,3-propanediol under the trade name Susterra® is produced by DuPont Tate & Lyle BioProducts and was used as a chain extender. This bio-based, petroleum-free chemical compound is manufactured via biotechnological process (fermentation) from corn sugar. The second non-petroleum based building block utilized in this research work is bio-based polypropanediol. Polypropanediol (PO3G) is produced by Allessa company through polycondensation of Susterra® propanediol. Chemically, bio-based polypropanediol is linear polyether polyol with three carbons in the polymer chain very similar to petroleum-based polytetramethylene ether glycol (PTMG).

In addition to replacing fuel-based platform chemicals with bio-based raw materials, the incorporating natural chemical compounds as filler in polymer composites is an important issue. Environmentally friendly bio-composites have the potential to be new products that respond to the current need for sustainable development and sensible resource management. In the case of bio-based polyurethane composites, nano- and micro- scale powders and fibers are used as a reinforcement, for example, chitin [23,24] and chitosan [25-27], silica [28], titanium dioxide [29], sisal

*Corresponding author: janusz.datta@pg.edu.pl

fibers [30], hydroxyapatite [31], lignin [32], kenaf fibers [33] and much more. Due to their advantageous characteristics, cellulose nanocrystals (CNC), nanofibrillated cellulose (NFC), microfibrillated cellulose (MFC), and microcrystalline cellulose (MCC) are also used as the reinforcing filler in the wide range of polymer composites. The hydroxyl units on the cellulose surface easily interact with the polymeric matrices, improving the fiber-matrix adhesion [34,35]. Microcrystalline cellulose (MCC), which was used as a filler, is a white, odourless form of cellulose, which is a naturally occurring compound from partially depolymerized and purified cellulose [36]. Properties of MCC are dependent on origin of the raw material (e.g. jute, cotton waste, bagasse and cob, bamboo, hulls, husks, nutshells, stalks, oil palm biomass, paper, cereal straw, sugar beet pulp etc.) and their extraction process [36-40].

In the present study, we attempted to design the method of synthesis the microcrystalline cellulose-filled poly(ether-urethane) composites with a high content of bio-based components. The final materials were thoroughly analyzed to evaluate the potential of microcrystalline cellulose at different content as a filler. The XRD technique has been used to assess the crystallinity of the used cellulosed and obtained products. The characteristic chemical groups in the structure of the composites was analyzed by means of Fourier Transform Infrared (FTIR) spectroscopy. The number of free and hydrogen-bonded carbonyl groups was determined based on the deconvolution of C=O band. Furthermore, the morphology (by SEM method), dynamic mechanical properties (by DMTA technique), thermal characteristic (by TGA technique) and mechanical properties (i.e. tensile strength and hardness) of the prepared materials were also determined.

Experimental

Materials

Microcrystalline cellulose (Alpha-Cel BH65), with the average fiber length of 50 micrometers, was purchased from International Fiber Corporation (Belgium). Thermoplastic polyurethanes were synthesized by using bio-based polytrimethylene ether glycol (PO3G, M_w=2000 g/mol) (Velvetol®, Allesa, Germany), 4,4'-diphenylmethane diisocyanate (MDI) (BorsodChem, Hungary), and bio-based 1,3-propanediol (PDO) (Susterra®, DuPont, Germany) as a chain extender, with 0.3 wt.% of 1,4-diazabicyclo[2.2.2] octane (DABCO) as a catalyst.

Synthesis

The synthesis of thermoplastic polyurethanes was realized by a two-step method. Prior to synthesis, PO3G was vacuum dried for 2 h at 95 °C. In the first step (Figure 1(a)), the prepolymer was synthesized through a reaction between bio-based polytrimethylene glycol and diisocyanate. The prepolymer reaction was carried out at 80 °C for 2 hours. The resulting prepolymer contained terminal isocyanate groups in the amount of 6 %, which has been determined by a titration method (in accordance with ISO 14896 standard). In the second step (Figure 1(b)), the prepolymer chains were extended by using bio-based 1,3-propanediol with 0.3 wt.% of 1,4-diazabicyclo[2.2.2]octane, and different amounts of microcrystalline cellulose (1, 3, 5 and 7 wt.%). Prior to being used, the cellulose powder was dried out at 100 °C to achieve the constant mass. Finally, the prepared poly(ether-urethane)s and their composites were molded and cured at 100 °C for 24 hrs in a laboratory oven, which has completed the reaction. The prepared materials were synthesized at the [NCO]/[OH]

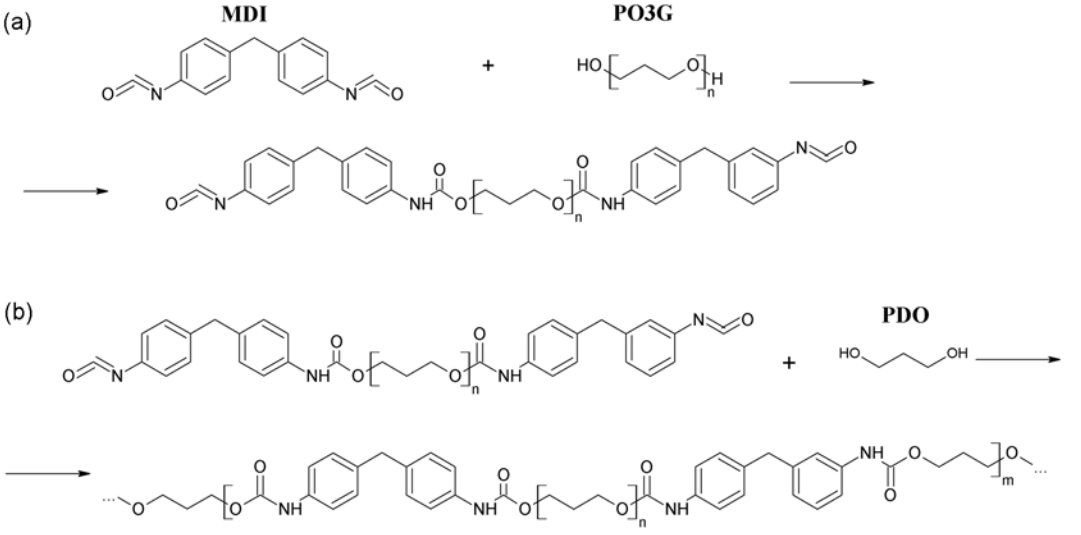

Figure 1. (a) Synthesis of polyurethane prepolymer through the reaction between diisocyanate (MDI) and bio-based polyol (PO3G) and (b) synthesis of poly(ether-urethane) through the reaction between prepolymer and bio-based chain extender (PDO).

molar ratio of 1.0.

By varying the content of cellulose (i.e. 1, 3, 5 and 7 wt.%), a series of composites was prepared and coded as TPU-1, TPU-3, TPU-5, TPU-7, respectively. The thermoplastic polyurethane matrix was coded as TPU.

Methods

Fourier Transform Infrared Spectroscopy (FTIR)

The FTIR analysis was carried out using a FTIR Nicolet 8700 spectrophotometer (Thermo Electron Corporation) and the ATR (Heated Golden Gate from Specac Ltd.) technique. The chemical structure of the prepared poly(ether-urethane) composites was assessed at room temperature for wavenumbers between 500 and 4000 cm^{-1}, with a resolution of 4 cm^{-1}. Each spectrum was acquired with 64 scans. In order to calculate the carbonyl hydrogen-bonding index, the deconvolution of spectra in the carbonyl region was carried out using Origin software.

$$R = \frac{A_{1703}}{A_{1730}}$$

where, R: carbonyl hydrogen bonding index, A_{1703}: intensity of the characteristic absorbance of hydrogen-bonded carbonyl, A_{1730}: intensity of the characteristic absorbance of free carbonyl groups

X-ray Diffraction (XRD)

In order to determine the structural properties of obtained materials, Phillips X'Pert Pro diffractometer (XRD) with CuK_{α} radiation (1.540 Å) was used. The measurements were carried out at 40 kV and 30 mA at room temperature. The diffraction angle of 2θ ranged from 10 ° to 70 °.

Scanning Electron Microscopy (SEM)

The microstructure of the cross-sections of prepared poly(ether-urethane)s and their composites were investigated using Scanning Electron Microscopy (SEM Phenom G2 PRO). The analyzed polyurethane samples were coated with gold prior to microscopic observations. The surface morphology was investigated at different magnifications to observe the dispersion of filler and the filler interaction with the poly(ether-urethane) matrix. Dimensions of the analyzed samples were typically 3 mm×3 mm. Each sample was cut with a scalpel in one quick motion.

Thermogravimetric Analysis (TGA)

Thermogravimetric analysis (TGA) of prepared poly(ether-urethane)s and their composites were performer using NETZSCH TG 209F1 Libra analyzer. The samples were heated from 25 to 600 °C at a rate of 10 °C/min. The measurements were realized under nitrogen atmosphere. The samples mass was around 10 mg.

Dynamic Mechanical Thermal Analysis (DMTA)

The dynamic mechanical analysis of bio-based poly(ether urethane)s and their composites containing powdered cellulose was performed by using a DMTA Q800 Analyzer (TA Instruments) under a nitrogen atmosphere. The measurements were taken in the temperature range from -100 to 150 °C at an operating frequency of 10 Hz, with a heating rate of 4 °C/min. The variation of storage modulus, loss modulus and tangent delta versus temperature was determined. The samples dimensions were 10 mm wide, 2 mm thick and 40 mm long. DMTA was performed under flexure.

Tensile Test

Static tensile properties (tensile strength and elongation at break) was carried out by using a Zwick Z020 tensile-testing machine with cross-head speed 100 mm/min. The dumbbell-shaped samples with the dimension of 115 mm were analysed. The original gauge length (l_0) was equal 25 mm. The measurement was determined according to the ISO 527-1:1996 standard at the room temperature. For each prepared materials five independent tests were taken.

Hardness

Hardness was determined according to ISO 868:2005 standard by using an electronic Shore type D durometer (Zwick, Germany). Circle-shaped samples with a diameter of 56 mm were prepared. For each sample, 10 points of measurements were taken.

Density

Density was measured according to the ISO 2781 standard with using an analytical balance RADWAG by hydrostatics medium. The measurements were performed in methanol at 23 +/- 2 °C. The results are averaged from five independent tests for each prepared material.

Results and Discussion

Fourier Transform Infrared Spectroscopy

The obtained spectra of microcrystalline cellulose is shown in Figure 2. The broad absorption band observed at ca. 3660-3000 cm^{-1} is associated with the hydrogen bonded O-H stretching vibration between glucose units from α-cellulose and the peak at 2904 cm^{-1} appeared due to C-H asymmetric and symmetric stretching vibration [41]. The band at 1638 cm^{-1} is related to the vibration of absorbed water molecules due to an interaction between water and cellulose [42]. The maximum at 1428 cm^{-1} is assigned to a $-CH_2$ bending and wagging vibration and is known as the crystallinity band. The intensity of this peak indicates the degree of cellulose crystallinity [43,44]. The absence of peaks in the range from ca. 1500 to 1600 cm^{-1} corresponds to C=C aromatic skeletal vibrations suggest that lignin was removed completely. In addition, peaks in the region from 1700 to 1740 cm^{-1} would normally indicate the presence of hemicelluloses, but do not occur on the obtained spectrum [42]. The absorbance at 1374 cm^{-1} arises from the O-H bending vibration and this at 1310 cm^{-1} is attributable to C-C and C-O groups of aromatic ring skeletal vibrations. The peak at 1155 cm^{-1} corresponds to the C-O-C stretching of the β-1,4-glycosidic linkage in cellulose chemical structure [45].

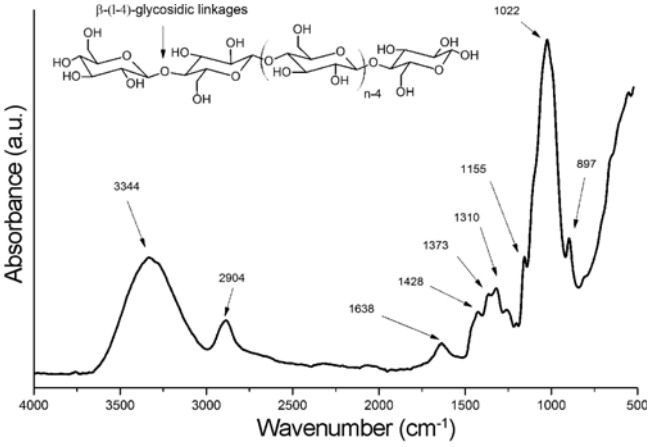

Figure 2. FTIR spectra of microcrystalline cellulose (MCC).

The pyranose ring skeletal vibration (C-O-C) is also registered at 1022 cm^{-1} [41,46]. C-H asymmetric out of plane ring stretching, which are characteristic for cellulose due to β-glycosidic linkage as well as amorphous form present in the structure are appeared at 897 cm^{-1} [36,41,42,46].

On the basis of FTIR spectra, the total crystallinity index (TCI) of used microcrystalline cellulose was calculated according to following formula:

$$R_c = A_{1373}/A_{2904}$$

where, A_{1373}: absorbance ratio from 1373 cm^{-1}, A_{2904}: absorbance ratio from 2904 cm^{-1}. The total crystallinity index determined for the used microcrystalline cellulose is 95.91 %.

In general, the spectra of poly(ether-urethane)s and poly(ether-urethane) composites presented in Figure 3 were very similar. The obtained spectra of thermoplastic polyurethanes did not display the stretching vibrations of the isocyanate group (N=C=O) at 2270 cm^{-1}, thus all of the isocyanate groups reacted during the polymerization process (Figure 3(a)). The stretching vibrations of N-H bond in the urethane group ware registered at 3320 cm^{-1}. As can be seen in Figure 3(b), the cellulose addition resulted in the adsorption band shifting and band intensity variation. The stretching vibrations of NH- groups at approximately 3320 cm^{-1} showed the highest absorption intensity for TPU-7, and the lowest absorption intensity for TPU [47,48]. Thus, the intensity of NH stretching vibrations increased with increasing cellulose concentration. Furthermore, with the increasing content of cellulose per sample, the band corresponding to the N-H bond became progressively wider, and it shifted to higher wavenumbers (Figure 3(b)) [48,49]. According to the available literature, the infrared bands

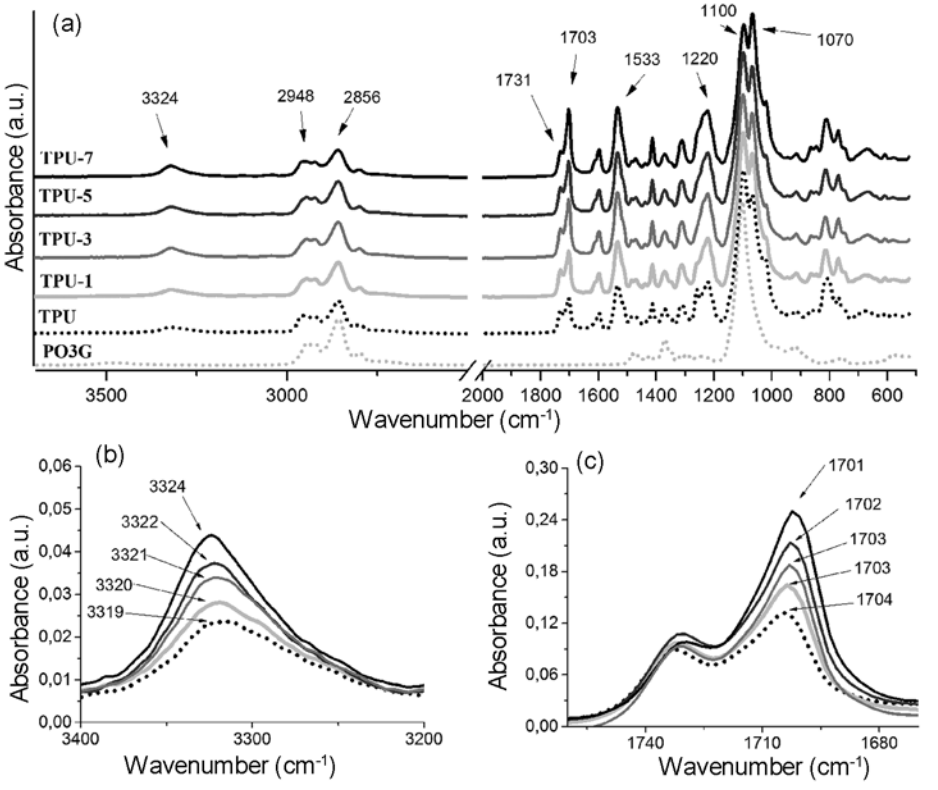

Figure 3. (a) Normalized FTIR spectra of the prepared thermoplastic polyurethanes and their composites, (b) FTIR spectra in the range 3400-3200 cm^{-1}, and (c) in the range 1780-1660 cm^{-1}.

Table 1. Location, fraction of curve fitting peaks for the -C=O band and the carbonyl hydrogen bonding index in the FTIR spectra of the composites with cellulose

Sample code	-C=O band				$R=A_{1703}/A_{1730}$
	Peak I: Free C=O		Peak II: Hydrogen bonded C=O		
	Location (cm^{-1})	Fraction (%)	Location (cm^{-1})	Fraction (%)	
TPU	1731.57	35.62	1703.67	64.38	1.541
TPU-1	1731.34	35.36	1703.50	64.64	1.725
TPU-3	1731.21	33.76	1703.18	66.24	2.070
TPU-5	1730.88	28.76	1702.21	71.24	2.741
TPU-7	1730.44	27.36	1701.47	72.64	2.802

observed at ca. 3320 cm^{-1} indicate that the hydrogen-bonded N-H groups are present in the polyurethane sample [50]. The peak we observed at 1533 cm^{-1} corresponds to the C-N stretching vibrations. The double peak in the range from 1680 to 1740 cm^{-1} is attributable to the stretching vibrations of C=O groups that are present in the structure of the urethane bond [51]. The maximum observed at 1704 cm^{-1} is associated with the hydrogen-bonded carbonyl groups in the ordered crystalline regions. According to the published reports, the segmented thermoplastic polyurethanes obtained by using MDI display the absorbance band at 1685-1706 cm^{-1} in the ordered crystalline regions, and at 1713-1718 cm^{-1} in the less ordered amorphous region [52,53]. The FTIR spectra have been normalized so as to show the relative intensity differences between the hydrogen-bonded and free carbonyl groups. In addition, the intensities of individual spectra were determined by the deconvolution of the FTIR spectra. Thus, the carbonyl hydrogen-bonding index (R) was estimated, namely, the intensity ratio of the hydrogen-bonded C=O band to the free C=O band (Table 1). The data presented in Figure 3(c) and Table 1 show that the intensity and fraction of the characteristic band of the hydrogen-bonded carbonyl groups (1703 cm^{-1}) increased with increasing cellulose concentration. A similar phenomenon was reported by other authors [49]. Additionally, the carbonyl hydrogen-bonding index increased with increasing cellulose content. Specifically, the value of R increased from 1.541 for TPU to 2.802 for TPU-7, which indicates an enhancement in the proportion of hydrogen-bonded C=O groups with increasing filler concentration [54]. The maximum at 1730 cm^{-1} is connected to the presence of free carbonyl groups; the peak intensity slightly changes with changing cellulose content (Table 1) [51]. The carbonyl hydrogen-bonding index increased with increasing values of cellulose content. Based on the available literature, this finding can be explained by the lack of covalent bonding between cellulose and polyurethane. The limited mobility and ability to bind hydrogen by cellulose can be observed in the case of materials with covalent bonding between the filler and matrix. As a result, cellulose acts as a crosslinking agent, and it improves the thermo-mechanical properties and thermal stability of the composite material [54,55]. Moreover, it was reported that the high number of hydrogen bonds could not possibly have resulted from the strong hydrogen bonds between the filler and the polymeric matrix, but rather from the chemical structure of cellulose particles [48]. In this study, the infrared bands in the region between 2800 cm^{-1} and 3000 cm^{-1} are attributable to the stretching vibrations of C-H groups. The PO3G polyol displayed the band at 1100 cm^{-1} that was assigned to the free C-O-C ether bond. The samples assigned to this particular region were characterized by the presence of a double peak.

The band observed at higher wavenumbers is characteristic for the C-O-C stretching vibrations, whereas the band with a maximum at 1070 cm^{-1} is connected to the ether groups that are hydrogen-bonded to the N-H bonds of the urethane groups; the intensity of the latter band increases with increasing cellulose content in the prepared materials [56,57].

X-ray Diffraction

X-ray diffraction (XRD) patterns for microcrystalline cellulose and prepared materials are shown in Figure 4. XRD patterns of microcrystalline cellulose fibers with the

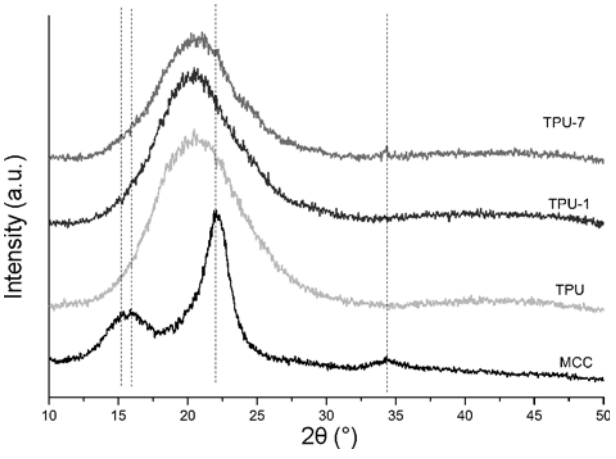

Figure 4. X-ray diffractograms of MCC and obtained polyurethane materials.

main diffraction signals at 2θ 15.2 °, 16.0 °, 22.1 ° and 34.4 ° correspond to the crystalline form. A typical crystal lattice of cellulose type I was observed [51].

The crystallinity index (Cr.I.) was calculated from the X-ray diffractions patterns according to following formula [58]:

$$\text{Cr.I. } (\%) = (Sc/St) \times 100$$

where, *Sc*: area of the crystalline domain, *St*: area of the total domain

The crystallinity index of MCC obtained from XRD patterns was 90 %.

In the case of TPU-1, peaks assigned to cellulose were invisible, because of the low content of MCC. Nevertheless, with an increase content of cellulose, materials exhibited two diffraction peaks. The diffraction peaks at about 2θ 22.1 ° and 34.4 ° for TPU_7 confirmed the presence of MCC in prepared materials. This suggests that the original structure of cellulose was well maintained in the prepared composites [51].

Scanning Electron Microscopy

The dispersion of microcrystalline cellulose within the polyurethane matrix was studied by scanning electron microscopy. In Figure 5, the cross-sectional SEM images of surface morphology of both pure poly(ether-urethane)s and the composites filled with 1, 3, 5, and 7 wt.% of cellulose fibers are compared. The presence of cellulose in the polymeric matrix can be easily identified as white dots, which are noticeable in the SEM images of all prepared materials. The number of dots increased with increasing cellulose content in the prepared composites. The poly(ether-urethane) matrix can be seen as a dark region [40]. In the case of the materials with a low microcrystalline-cellulose content, i.e. 1 and 3 wt.% a homogeneous structure was observed that was comparable to that of pure polyurethane [49,59]. On the other hand, the added cellulose fibers adhered to the matrix in most cases. At high fiber loading, the cellulose particles were poorly distributed throughout the polyurethane matrix. The single cellulose particles were observed; they also tended to form aggregates. The very large clusters of filler have not been observed, however, the forming clusters were increasingly larger with increasing cellulose content (see Figure 6). The slightly poorer interfacial adhesion and worse interactions between the dispersed bio-filler and the matrix were confirmed based on the presence of gaps between the filler and the matrix [60]. The observed gaps, agglomerates and dimples may form due to incompatibility between the hydrophobic and non-polar polymer matrix and hydrophilic and polar fibers [36]. This phenomenon could have an effect on the deterioration of the mechanical properties of produced polyurethanes.

Thermogravimetric Analysis

The thermogravimetric analyses enable to characterize the thermal stability of the polyurethane samples. The analysis results of the prepared materials are listed in Table 2. Figure 7 presents the TGA and DTG curves of the microcrystalline cellulose and obtained samples. The TGA curve obtained for the MCC displays three different weight losses [61]. The

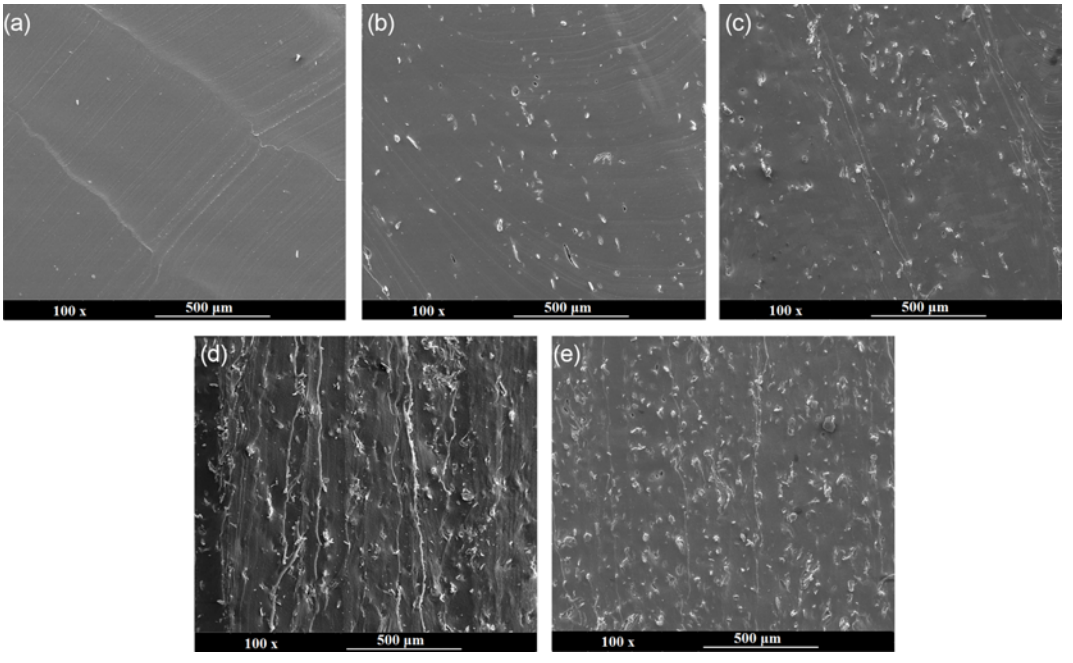

Figure 5. Typical cross-section SEM images of (a) poly(ether-urethane)s matrix (TPU), and their composites with (b) 1 wt.%, (c) 3 wt.%, (d) 5 wt.%, and (e) 7 wt.% microcrystalline cellulose.

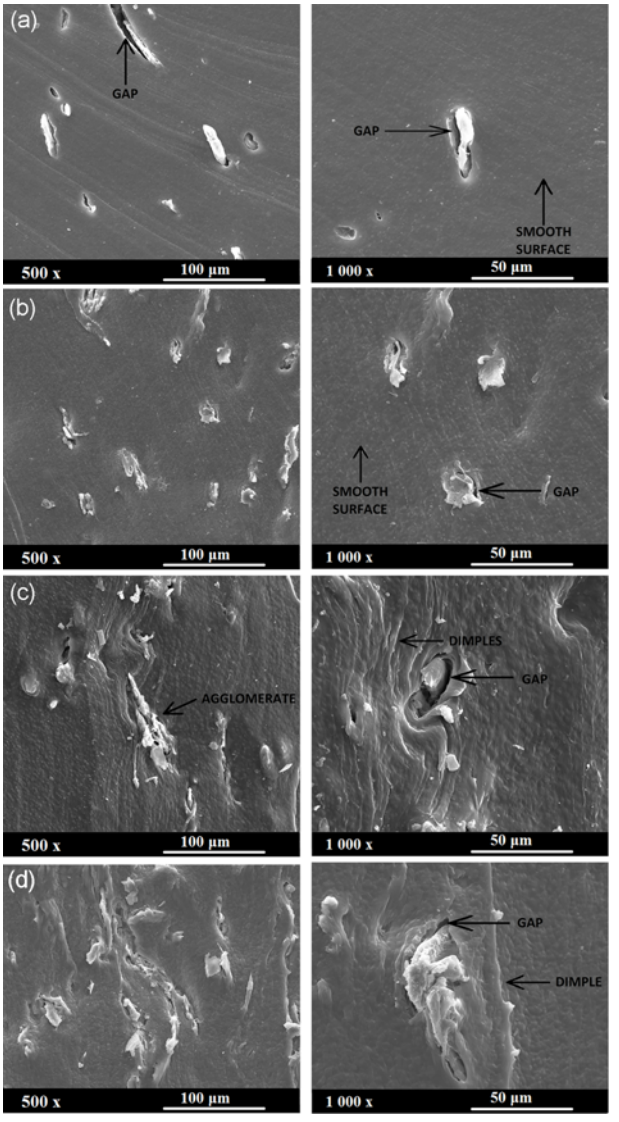

Figure 6. SEM micrographs of prepared composites with (a) 1 wt.%, (b) 3 wt.%, (c) 5 wt.%, and (d) 7 wt.% microcrystalline cellulose.

initial weight loss was occurred at temperature below 200 °C due to the evaporation and removal of water. The maximum weight loss was shown in the temperature range of 290 to 350 °C which was attributed to the thermal depolymerization of cellulose, hemicellulose, and lignin [62]. The third small weight loss over the temperature range 350 to 600 °C was associated with degradation of cellulose residues. The peak on the DTG curve was attributed to the maximum degradation temperature (T_{max}=353.6 °C) corresponding to the maximum

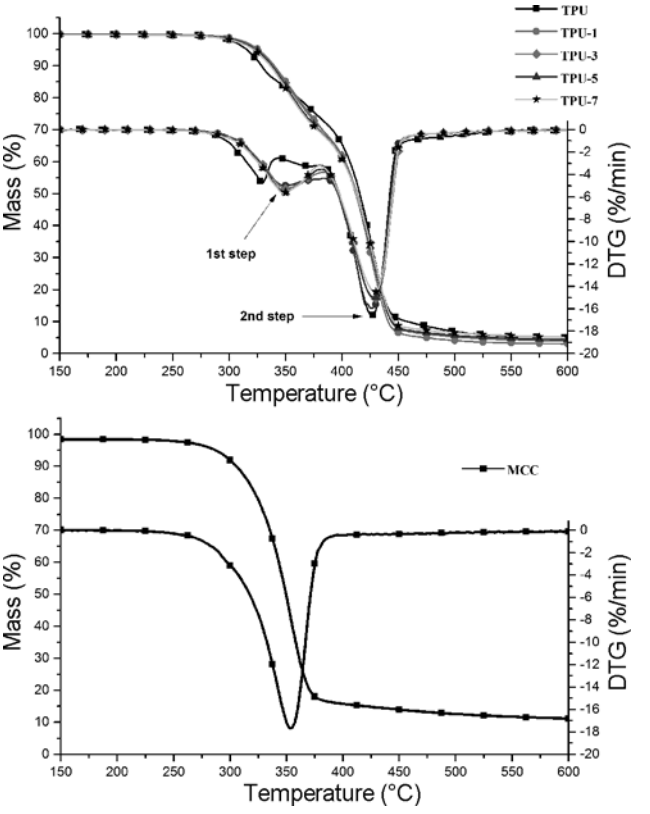

Figure 7. TGA and DTG curves of prepared materials and microcrystalline cellulose.

Table 2. Thermal stability of microcrystalline cellulose and obtained materials

Sample	$T_{5\%}$ (°C)	$T_{10\%}$ (°C)	$T_{50\%}$ (°C)	$T_{90\%}$ (°C)	Char residues at 600 °C (%)	TG/DTG		
						Step	T_{max} (°C)	DTG (%/min)
MCC	290.1	317.1	349.8	-	11.18	I	353.6	-17.53
TPU	315.5	328.7	415.8	458.1	3.01	I	329.3	-4.75
						II	426.4	-16.61
TPU-1	321.4	338.1	412.2	440.9	3.08	I	348.0	-4.99
						II	426.6	-15.86
TPU-3	323.2	337.6	413.4	444.3	3.93	I	348.8	-5.28
						II	428.4	-15.10
TPU-5	324.5	339.9	407.5	443.8	4.40	I	350.3	-5.60
						II	428.8	-15.02
TPU- 7	326.0	340.0	412.6	445.7	5.09	I	350.9	-5.68
						II	429.1	-14.42

rate of thermal decomposition of cellulose. The results present that the increasing content of MCC in the polyurethane sample has a beneficial impact on the thermal stability of prepared TPU. The higher temperatures of thermal decomposition are observed so thermal decomposition was improved with the increase in MCC content [63]. The TGA and DTG curves of prepared materials exhibit a two-step degradation process. The first step was occurred at the temperature range 300 to 350 °C and is referred to the decomposition of urethane hard segment linkages [64,65]. In the second step, the weight loss at the temperature range 400 to 450 °C corresponded to the degradation of soft segments. The degradation of the samples results in cleavage of the macromolecule chain structure. The onset temperatures during the first degradation step were higher for materials filled with MCC than for reference sample (Table 2). Therefore it was concluded that the addition of MCC increased the thermal decomposition temperatures corresponding to 5, 10, 50, and 90 % weight loss. The addition of cellulose caused a shift of T_{max} to the higher temperature in which the fastest loss in mass occurs for both the first and second step degradation. Noticeable increase in thermal stability resulting from the addition of MCC might be ascribed to the strong hydrogen bonding interaction between MCC and TPU, also proved by FTIR spectroscopy [66].

Dynamic Mechanical Thermal Analysis

The dynamic mechanical properties of poly(ether-urethane)s and their composites containing different cellulose levels were investigated by DMTA. The thermo-mechanical behavior of composites over a broad temperature range depends on the structure and morphology of the material. The obtained results are shown in Figures 8 and 9. The viscoelastic properties of the samples were related to the microdomain thermal transitions. The shape of the curves indicates that the addition of microcrystalline cellulose had a

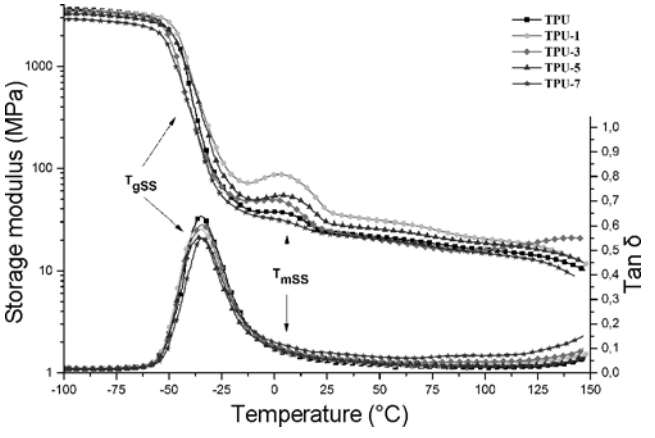

Figure 8. Temperature dependence of storage modulus and tan delta of the thermoplastic poly(ether-urethane) and their composites filled with microcrystalline cellulose.

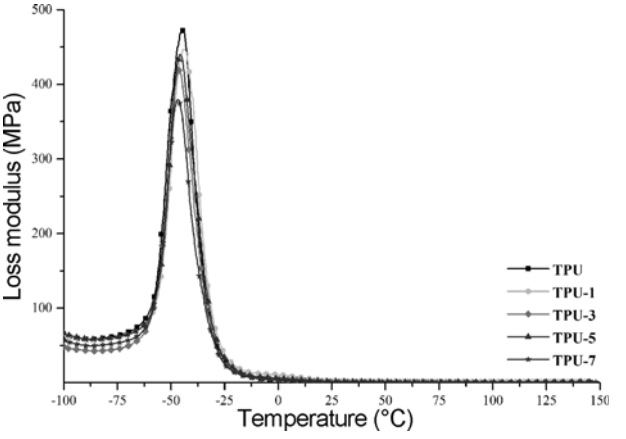

Figure 9. Temperature dependence on loss modulus of the thermoplastic poly(ether-urethane) and their composites filled with microcrystalline cellulose.

slight effect on the glass transition of the soft segment in all the examined samples. The registered curves for composites have a typical course as for neat polyurethane material. In the temperature range from ca. -50 °C to -25 °C, a decrease in the storage modulus was observed, which is associated with the glassy relaxation and glass transition temperature of the soft segment. Moreover, the storage modulus showed a decrease during the glass-rubber transition and kept decreasing in the rubbery region due to the thermoplastic nature of the material [51]. The consecutive transition is related to the melting of crystalline soft segments introduced by the ether-based polyol, which has also been reported in the literature [67-69]. The cellulose content had a slight influence on the course of curves and hence on the thermo-mechanical properties of obtained materials. An improvement in the storage modulus was achieved by introducing 1-5 wt.% cellulose into the TPU matrix. This is due to both cellulose reinforcement and increased cross-link density from the TPU-MCC interaction. The enhancement of mechanical properties observed in case of TPU-1, TPU-3, TPU-5 above T_g suggests the formation of rigid particle networks by the cellulose in the polymer matrix, where stress transfer is facilitated by hydrogen-bonding. Reinforcement has higher hardness than neat TPU, so the local stiffening of the material is created, which also results from hydrogen interaction. In the case of TPU-7, the improvement effect is not noticeable, because the filler-filler interactions are stronger than filler-TPU. This has also been confirmed during morphology analysis, where the formation of aggregates was observed. The maximum values of tan delta peaks were observed in the (0.63-0.54) range; they slightly decreased with the increasing content of the microcrystalline cellulose filler. At higher temperatures, the melting of soft segments was noticeable. The loss modulus of the prepared materials ranged from 379 to 471 MPa. The highest value of loss

modulus was observed for thermoplastic poly(ether-urethane)s (TPU) without the bio-filler. In the case of cellulose filler addition, a decrease in the loss modulus was found. It can be concluded that with the increasing content of MCC and formation of a cellulose network, Young's modulus of the composites increased. On the other hand, rigid polymer networks resulted in a decrease in elongation at break and tensile strength, which was observed during tensile strength tests.

Mechanical Properties

In Figure 10 the values of Young's modulus, elongation at break, and tensile strength of pure polyurethane and the derived composites are compared with respect to the percentage weight of microcrystalline cellulose added. The presented results show that the amount of microcrystalline cellulose has a significant effect on the mechanical properties of the prepared materials. Both tensile strength and elongation at break of the filled polyurethane composites decreased with increasing cellulose concentration. The cellulose loading, ranging from 1 to 5 wt.%, caused a small deterioration of mechanical properties. However, in the case of 7 wt.% filling, the mechanical properties decreased quite considerably. Due to the addition of cellulose powder, the tensile properties of composites decreased from 24.5 MPa to 8.6 MPa for TPU-1 and TPU-7, respectively. The incorporation of higher amounts of cellulose resulted in a decrease in the elongation at break, i.e. from 749 to 373 % for TPU-1 and TPU-7, respectively. The observed tendency can be possibly related to the filler agglomeration which, in turn, entails a limited transfer of load from the polymeric matrix to the filler due to the presence of cellulose clusters. The aforementioned phenomenon could initiate and then propagate the formation of cracks, which would reduce the tensile properties of the obtained composites [70]. In addition, poor interfacial adhesion and worsened interactions between the filler and the matrix can cause gaps in the material's structure, which will also adversely affect the tensile strength. Moreover, under the described scenario, the content of polymeric component will decrease, while the filler amount will increase, resulting in the reduced elongation at break. The addition of microcrystalline cellulose caused an increase in the value of Young's modulus of the final materials. This finding can be related to the increased stiffness of the obtained poly(ether-urethane)s. The results of tensile testing were consistent with the outcome of the dynamic mechanical analysis.

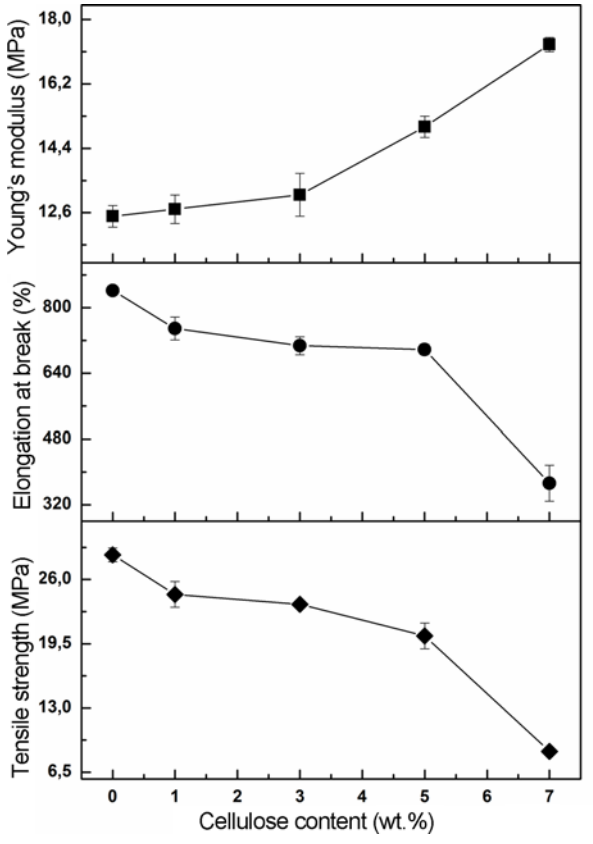

Figure 10. Mean values of Young's modulus, elongation at break and tensile strength polyurethane composites with respect to the weight percentage of microcrystalline cellulose.

The measured values of density and hardness for all prepared materials are summarized in Table 3. Based on the data analysis, it can be stated that the elevated levels of cellulose filler caused an increase in the material's hardness from 27.54 to 32.75 ^{o}ShD for TPU and TPU-7, respectively.

The density of the prepared materials also depended on the cellulose content in the composites. It was observed that the admixture of cellulose increased the density of the obtained thermoplastic poly(ether-urethane)s from 1.105 to 1.119 for TPU-1 and TPU-7, respectively. The obtained results suggest that the density of microcrystalline cellulose is higher than that of PU matrix.

Table 3. Density and hardness of thermoplastic poly(ether-urethane)s and their composites filled with microcrystalline cellulose

Properties	Code of samples				
	TPU	TPU-1	TPU-3	TPU-5	TPU-7
Hardness (^{o}Sh A)	80.49±0.28	82.27±0.31	83.39±0.23	83.63±0.29	84.79±0.44
Hardness (^{o}Sh D)	27.54±0.28	29.34±0.24	31.02±0.27	31.76±0.34	32.75±0.31
Density (g/cm^{3})	1.104±0.009	1.105±0.002	1.111±0.001	1.114±0.001	1.119±0.002

Conclusion

The presented work demonstrates that poly(ether-urethane)-based composites with satisfactory thermo-mechanical and thermal properties could be obtained using bio-components such as bio-based polyol (Velvetol®), bio-based glycol (Susterra® Propanediol) and different amount of microcrystalline cellulose (MCC). On the basis of FTIR spectra, the total crystallinity index of pure cellulose fibres amounted to 95.91 %. This index provided information about the ratio of crystalline (ordered) and amorphous (disordered) regions of cellulose. The XRD analysis demonstrated a typical crystal lattice of cellulose type I. The crystallinity calculated on the basis of XRD patterns amounted to 90 %. Noticeable increase in thermal stability with increasing amount of MCC might be ascribed to the strong hydrogen bonding interaction between MCC and TPU, which was also proved by FTIR spectroscopy. The glass transition was similar for all the thermoplastic poly(ether-urethane)s and bio-based composites derived from these TPUs. Despite the fact that the addition of cellulose microcrystalline influence on the hydrogen bond formation, the selected properties decrease with the increasing content of bio-filler. Moreover, the addition of bio-filler results in increasing of hardness, Young's modulus and material density. The SEM analysis demonstrated that the microcrystalline cellulose was homogeneously distributed in the polymeric matrix when small amounts of filler (1 and 3 wt.%) were applied. At higher fiber concentrations (5 and 7 wt.%), the cellulose particles were poorly distributed throughout the polyurethane matrix, and displayed a tendency for forming aggregates. The slightly poor interfacial adhesion and worse interactions between the dispersed filler and the polymeric matrix have been confirmed by the presence of gaps between the filler and the matrix. The obtained poly(ether-urethane)-based composites displayed the desired characteristic and, therefore, showed a wide range of industrial applications, offering the unique characteristics of microcrystalline cellulose as well as polyurethane. Furthermore, taking into account the issues of environmental protection and sustainable development, the sensible resource management and the application of bio-based building block chemicals in the polyurethane synthesis are desired. The whole presented study is a preliminary step towards the fully bio-based polyurethane composites with microcrystalline cellulose. In the future, it will be necessary to improve adhesion between the filler and polyurethane matrix, which will have an impact on the better material properties. In order to improve the interfacial adhesion, the surface properties should be improved appropriately. One of the possibilities is physical treatments such as corona treatment, plasma treatment or electron beam irradiation. Another solution is chemical treatments such as alkaline treatment, acetylation, benzoylation, peroxide or silane treatment, and maleated coupling agents treatments.

References

1. G. Lligadas, J. C. Ronda, M. Galia, and V. Cadiz, *Materials Today*, **16**, 337 (2013).
2. K. Błażek and J. Datta, *Critical Rev. Environ. Sci. Technol.*, **49**, 173 (2019).
3. J. Datta, M. Łaski, and J. Kucinska-Lipka, *Przemysł Chemiczny*, **86**, 63 (2007).
4. J. Datta and P. Kasprzyk, *Polym. Eng. Sci.*, **58**, E14 (2017).
5. J. Datta and A. Balas, *J. Therm. Anal. Calorim.,* **74**, 615 (2003).
6. N. E. Marcovich, M. Kurańska, A. Prociak, E. Malewska, and K. Kulpa, *Ind. Crops Prod.*, **102**, 88 (2017).
7. M. Kurańska, and A. Prociak, *Ind. Crops Prod.*, **89**, 182 (2016).
8. M. A. Mosiewicki, P. Rojek, S. Michałowski, M. I. Aranguren, and A. Prociak, *J. Appl. Polym. Sci.*, **132**, 1 (2015).
9. A. Hejna, M. Kirpluks, P. Kosmela, U. Cabulis, J. Haponiuk, and Ł. Piszczyk, *Ind. Crops Prod.*, **95**, 113 (2017).
10. A. Palanisamy, M. S. L. Karuna, T. Satyavani, and D. B. Rohini Kumar, *J. Am. Oil Chemists' Society*, **88**, 541 (2011).
11. W. Liu, K. Xu, C. Wang, B. Qian, Y. Sun, Y. Zhang, H. Xie, and R. Cheng, *J. Therm. Anal. Calorim.*, **123**, 2459 (2016).
12. R. Surender, A. R. Mahendran, G. Wuzella, and C. T. Vijayakumar, *J. Therm. Anal. Calorim.*, **123**, 525 (2016).
13. X. Kong, G. Liu, and J. M. Curtis, *Eur. Polym. J.*, **48**, 2097 (2012).
14. L. K. Jia, L. X. Gong, W. J. Ji, and C. Y. Kan, *Chinese Chem. Lett.*, **22**, 1289 (2011).
15. Ł. Piszczyk, M. Strankowski, M. Danowska, A. Hejna, and J. T. Haponiuk, *Eur. Polym. J.*, **57**, 143 (2014).
16. C. M. Obele, O. Ogbobe, and I. F. Okonkwo, *Pakistan J. Nutricion*, **9**, 1058 (2010).
17. A. Drozdzyńska, K. Leja, and K. Czaczyk, *J. Biotechnol. Comput. Biol. Bionanotechnol.*, **92**, 92 (2011).
18. S. Joshi and V. Ranade in "Industrial Catalytic Processes for Fine and Specialty Chemicals" (P. Kumbhar, J. Sawant, and A. Ghosalkar Eds.), pp.597-662, Elsevier, 2016.
19. B. Erickson, Nelson, and P. Winters, *Biotechnol. J.*, **7**, 176 (2012).
20. L. Hojabri, X. Kong, and S. S. Narine, *Biomacromolecules*, **10**, 884 (2009).
21. A. S. More, T. Lebarbé, L. Maisonneuve, B. Gadenne, C. Alfos, and H. Cramail, *Eur. Polym. J.*, **49**, 823 (2013).
22. T. Calvo-Correas, A. Santamaria-Echart, A. Saralegi, L. Martin, Á. Valea, M. A. Corcuera, and A. Eceiza, *Eur. Polym. J.*, **70**, 173 (2015).
23. K. Mahmood, K. M. Zia, W. Aftab, M. Zuber, S. Tabasum, A. Noreen, and F. Zia, *Int. J. Biol. Macromol.*, **113**, 150 (2018).
24. K. Mahmood, K. M. Zia, M. Zuber, S. Tabasum, S. Rehman, F. Zia, and A. Noreen, *Int. J. Biol. Macromol.,* **105**, 1180 (2017).

25. A. Usman, K. M. Zia, S. Tabasum, S. Rehman, and F. Zia, *Int. J. Biol. Macromol.,* **86**, 630 (2016).
26. M. A. Javaid, R. A. Khera, K. M. Zia, K. Saito, I. A. Bhatti, and M. Asghar, *Int. J. Biol. Macromol.,* **115**, 375 (2018).
27. R. da Rosa Schio, B. C. da Rosa, J. O. Gonçalves, L. A. A. Pinto, E. S. Mallmann, and G. L. Dotto, *Int. J. Biol. Macromol.,* **121**, 373 (2019).
28. S. Das, P. Pandey, S. Mohanty, and S. K. Nayak, *Int. Biodeterior. Biodegrad*., **117**, 278 (2017).
29. V. D. Da Silva, L. M. Dos Santos, S. M. Subda, R. Ligabue, M. Seferin, C. L. P. Carone, and S. Einloft, *Polym. Bull.*, **70**, 1819 (2013).
30. E. Głowińska, J. Datta, and P. Parcheta, *J. Therm. Anal. Calorim*., **130**, 113 (2017).
31. L. P. Gabriel, M. E. M. dos Santos, A. L. Jardini, G. N. T. Bastos, C. G. B. T. Dias, T. J. Webster, and R. Maciel Filho, *Biol. Med.*, **13**, 201 (2017).
32. C. Zhang, H. Wu, and M. R. Kessler, *Polymer*, **69**, 52 (2015).
33. J. Datta and P. Kopczyńska, *Ind. Crops Prod.*, **74**, 566 (2015).
34. M. A. Mosiewicki, U. Casado, N. E. Marcovich, and M. I. Aranguren, *Polym. Eng. Sci.*, **49**, 685 (2009).
35. Z. Rafiee and V. Keshavarz, *Prog. Org. Coat.,* **86**, 190 (2015).
36. D. Trache, M. H. Hussin, C. T. Hui Chuin, S. Sabar, M. R. N. Fazita, O. F. A. Taiwo, T. M. Hassan, and M. K. M. Haafiz, *Int. J. Biol. Macromol.,* **93**, 789 (2016).
37. A. Cataldi, A. Dorigato, F. Deflorian, and A. Pegoretti, *J. Mater. Sci*., **49**, 2035 (2014).
38. X. Kong, L. Zhao, and J. M. Curtis, *Carbohydr. Polym.*, **152**, 487 (2016).
39. A. Santamaria-Echart, L. Ugarte, C. García-Astrain, A. Arbelaiz, M. A. Corcuera, and A. Eceiza, *Carbohydr. Polym.,* **151**, 1203 (2016).
40. Q. Zhao, G. Sun, K. Yan, A. Zhou, and Y. Chen, *Carbohydr. Polym.,* **91**, 169 (2013).
41. A. M. Adel and N. A. El-shinnawy, *Int. J. Biol. Macromol.,* **51**, 1091 (2012).
42. M. K. M. Haafiz, A. Hassan, Z. Zakaria, and I. M. Inuwa, *Carbohydr. Polym.*, **103**, 119 (2014).
43. D. Trache, M. H. Hussin, C. T. Hui Chuin, S. Sabar, M. R. N. Fazita, O. F. A. Taiwo, T. M. Hassan, and M. K. M. Haafiz, *Int. J. Biol. Macromol.*, **93**, 789 (2016).
44. R. D. Kalita, Y. Nath, M. E. Ochubiojo, and A. K. Buragohain, *Colloids and Surfaces B: Biointerfaces*, **108**, 85 (2013).
45. K. Das, D. Ray, N. R. Bandyopadhyay, and S. Sengupta, *J. Polym. Environ.*, **18**, 355 (2010).
46. A. M. Adel, Z. H. Abd El-Wahab, A. A. Ibrahim, and M. T. Al-Shemy, *Carbohydr. Polym.*, **83**, 676 (2011).
47. Y. A. El-Shekeil, S. M. Sapuan, A. Khalina, E. S. Zainudin, and O. M. Al-Shuja'a, *Express Polym. Lett.*, **6**, 1032 (2012).
48. H.-Y. Mi, X. Jing, M. R. Salick, T. M. Cordie, and L.-S. Turng, *J. Mech. Behav. Biomed. Mate.,* **62**, 139 (2016).
49. A. Hadjadj, O. Jbara, A. Tara, M. Gilliot, F. Malek, E. M. Maafi, and L. Tighzert, *Compos. Struct.*, **135**, 217 (2016).
50. Y. I. Tien and K. H. Wei, *Polymer*, **42**, 3213 (2001).
51. S. Lin, J. Huang, P. R. Chang, S. Wei, Y. Xu, and Q. Zhang, *Carbohydr. Polym.*, **95**, 91 (2013).
52. H. D. Kim, T. J. Lee, J. H. Huh, and D. J. Lee, *J. Appl. Polym. Sci.*, **37**, 345 (1999).
53. T. L. Yu, T. L. Lin, Y. M. Tsai, and W. J. Liu, *J. Polym. Sci. Part B: Polym. Phys.*, **37**, 2673 (1999).
54. X. Kong, L. Zhao, and J. M. Curtis, *Carbohydr. Polym.,* **152**, 487 (2016).
55. A. Pei, J. M. Malho, J. Ruokolainen, Q. Zhou, and L. A. Berglund, *Macromolecules*, **44**, 4422 (2011).
56. L. Ugarte, B. Fernández-d'Arlas, A. Valea, M. L. González, M. A. Corcuera, and A. Eceiza, *Polym. Eng. Sci.,* **54**, 2282 (2014).
57. P. N. Lan, S. Corneillie, E. Schacht, M. Davies, and A. Shard, *Biomaterials*, **17**, 2273 (1996).
58. D. Ciolacu, F. Ciolacu, and V. I. Popa, *Cellulose Chem. Technol.*, **45**, 13 (2011).
59. Y. A. El-Shekeil, S. M. Sapuan, and M. W. Algrafi, *Mater. Des.*, **64**, 330 (2014).
60. M. Bassyouni, S. A. Sherif, M. A. Sadek, and F. H. Ashour, *Compos. Part B: Eng.*, **43**, 1439 (2012).
61. P. Khawas and S. C. Deka, *Carbohydr. Polym.*, **137**, 608 (2016).
62. H. Yang, R. Yan, H. Chen, D. H. Lee, and C. Zheng, *Fuel*, **86**, 1781 (2007).
63. A. I. Cordero, J. I. Amalvy, E. Fortunati, J. M. Kenny, and L. M. Chiacchiarelli, *Carbohydr. Polym.*, **134**, 110 (2015).
64. P. Alagi, Y. J. Choi, and S. C. Hong, *Eur. Polym. J.*, **78**, 46 (2016).
65. E. Głowińska and J. Datta, *Cellulose*, **23**, 581 (2016).
66. W. Lei, X. Zhou, C. Fang, Y. Song, and Y. Li, *Carbohydr. Polym.*, **209**, 299 (2019).
67. M. Włoch, J. Datta, and K. Błażek, *J. Polym. Environ.*, **4**, 4415 (2018).
68. C. Prisacariu, E. Scortanu, A. Airinei, B. Agapie, M. Iurzhenko, and Y. P. Mamunya, *Procedia Engineering*, **10**, 446 (2011).
69. L. S. T. J. Korley, B. D. Pate, E. L. Thomas, and P. T. Hammond, *Polymer (Guildf)*, **47**, 3073 (2006).
70. J. Ervina, M. Mariatti, and S. Hamdan, *Procedia Chemistry*, **19**, 897 (2016).